Biomass forest modelling using UAV LiDAR data under fire effect

Andreas Paul Adolf Bayer

Dissertação para obtenção do Grau de Mestre em

Engenharia Florestal e dos Recursos Naturais

Orientadores: Professora Ana Paula Soares Marques de Carvalho

Professor João Manuel das Neves Silva

Júri:

Presidente: Doutor, Maria da Conceição Brálio de Brito Caldeira, Professor Auxiliar do(a) Instituto Superior de Agronomiada Universidade de Lisboa.

Vogais: Doutor, Manuel Lameiras de Figueiredo Campagnolo, Professor Associado do(a) Instituto Superior deAgronomia da Universidade de Lisboa.

Doutor, João Manuel das Neves Silva, Professor Auxiliar do(a) Instituto Superior de Agronomia daUniversidade de Lisboa, orientador.

2019

ABSTRACT

The main goal of the study is to analyse the possibility of quantifying the loss of biomass in burned forest stands using Light Detection and Ranging (LiDAR) data. Since wildfires are not uncommon in Mediterranean areas, it is useful to quantify the magnitude of fire damage in forests. With the use of remote sensing, it is possible to plan post-fire recovery management and to quantify the losses of biomass and carbon stock. Mata Nacional de Leiria (MNL) was chosen, because, after the fire in October 2017, it showed areas with low and medium-high fire severity. MNL is divided in several rectangular management units (MU). To achieve our objective, it was necessary to find a MU with burned and unburned areas. In this selection process, we used Sentinel-2 images. The fire severity was estimated by deriving a spectral index related with the effects of fire and to compute the temporal difference (pre- minus post-fire) of this index, the delta normalized burn ratio (DNBR). Forest inventory was carried out in four plots installed in the selected MU. Allometric equations were used to estimate values of stand aboveground biomass. These values were used to fit a relationship with data extracted from LiDAR cloud metrics. The LiDAR data were acquired with a VLP-16 Velodyne LiDAR PUCK™ mounted on an Unmanned Aerial Vehicles (UAV) at an altitude of 60 m above the ground. The point clouds were then processed with the FUSION software until a cloud metrics was generated and then regression models were used to fit equations related to LiDAR-derived parameters. Two biomass equations were fit, one with the whole tree metrics having a R^2 = 0,95 and a second one only considering the tree crown metrics presenting a R^2 = 0,93. The state of the forest (unburned/burned) was significant on the final equation.

Keywords: Wildfires, Remote Sensing, Fire severity, Biomass loss, Maritime pine

ABSTRACT PORTUGUESE

Os impactos dos fogos florestais são alarmantes. Regiões com características diferentes são afetadas, verificando-se em algumas o avanço do fogo até às áreas urbanas, com prejuízo em residências e infraestruturas. Por outro lado, o fogo também é um fenómeno natural, tendo uma função importante nos ecossistemas. Nas áreas florestais não atingidas pelo fogo regularmente, a vegetação do sub-bosque acumula-se criando condições propícias à propagação de fogos severos. A avaliação dos danos na floresta provocados pelo fogo pode ser difícil pois é feita por avaliações no terreno. Esta avaliação é essencial para permitir avaliar o grau de severidade dos fogos nos ecossistemas florestais, ou seja, o seu impacte na vegetação e solo. Através da deteção remota é possível quantificar a perda de biomassa nos provoamentos florestais e planear a gestão da recuperação pós-fogo. O objetivo deste trabalho é analisar a possibilidade de quantificar a perda de biomassa em áreas ardidas de povoamentos florestais utilizando dados de Light Detection And Ranging (LiDAR).

A Mata Nacional de Leiria (MNL) foi escolhida pela sua importância a nível nacional e pelo facto de ter em ardido cerca de 9000 ha em apenas 2 horas do dia 17 de outubro de 2017. Os fogos na região apresentaram severidade baixa a média-alta e resultaram em uma floresta pós fogo com características particulares. A MNL está dividida em várias unidades de gestão (talhões). A seleção do talhão de estudo foi realizada de acordo com o mapa de severidade do fogo, obtido a partir de imagens do satélite Sentinel-2. Quatro parcelas de inventário de 20 x 20 m (400 m²) foram instaladas, com um total de 148 árvores de *pinus pinaster*, 75 em parcelas não-ardidas e 73 em parcelas ardidas. Foram medidas as posições das árvores, bem como a altura e o diâmetro a 1,30 m. Nas áreas não-ardidas a altura da base da copa de todas as árvores também foi medida. A biomassa das várias componentes da árvore foi estimada com equações alométricas e a biomassa acima do solo por hectare resultou na soma das biomassas das árvores das parcelas.

As utilização de imagens pós e pré-fogo do satélite Sentinel-2 permitiu elaborar a cartografia da severidade de fogo, através do cálculo do índice *Difference Normalized Burn Ratio* (DNBR).

Os dados do LiDAR foram adquiridos com o VLP-16 Velodyne LiDAR PUCK™ acoplado num *Unmanned Aerial Vehicle* (UAV) entre maio e junho de 2018, voando a uma altitude de 60 m acima do nível do solo. Durante o voo, o systema LiDAR foi configurado para varrer a área com uma abertura de ±35° relativamente ao nadir e armazenar até dois retornos por pulso (primeiro e último retorno). A trajetória de voo foi planeada para permitir uma sobreposição de 50% da cobertura varrida. Após o voo, os dados foram processados para obtenção das métricas do LiDAR. O processamento foi efetuado no programa FUSION

v.3.4.2. Foi realizada a filtragem dos pontos do terreno, a geração dos modelos digitais de terreno (*Digital Terrain Model*, DTM), a normalização dos dados em software R, e a extração das métricas da nuvem de pontos normalizada. O processamento dos dados do LiDAR resultou num conjunto de 102 métricas, que foram utilizadas para estimar a biomassa acima do solo. As equações selecionadas com três métricas do LiDAR resultaram de uma investigação exaustiva tendo como critério o valor mínimo da raíz quadrada do erro médio quadrático (RMSE). Além disso, foi adicionada ao modelo uma variável *dummy* relacionada com o status da parcela, isto é, ardida ou não ardida.

Os níveis do índice DNBR variaram de áreas não ardidas a severamente ardidas, revelando uma elevada variabilidade espacial. Em alguns locais, a distância entre áreas com fogo e com fogo não-severo foi inferior a 100 m. A separação entre áreas severamente atingidas e pouco atingidas pelo fogo foi claramente visível em campo, o que dá confiabilidade ao mapa de severidade baseado no DNBR. Nas áreas classificadas como não-ardidas no mapa de severidade não se observaram vestígios de fogos no campo, tanto nos troncos como nas copas das árvores.

Os dados do LiDAR apresentaram poucos pontos na superfície do terreno, especialmente nas áreas ardidas. Tal facto é devido à maior penetração dos feixes de laser em regiões onde as copas possuíam menos agulhas. Em muito casos, os troncos das árvores nas áreas queimadas estavam pretos até a base das copas. Já estas estavam castanhas devido à morte das agulhas provocada pelo fogo. O facto dos troncos serem pretos causou, possivelmente, interferências na reflectância dos feixes de laser do LiDAR.

A equação selecionada para a estimativa da biomassa incluiu as seguintes variáveis: altura máxima dos pontos, a assimetria da distribuição dos pontos e a altura relativa ao percentil 80%. Foram consideradas métricas extraídas dos pontos a 1 m acima do solo. A equação apresentou um bom ajustamento (R^2=0,94). Baseado nos resultados desta primeira estimativa da biomassa, foi ajustada outra equação considerando métricas extraídas dos pontos acima de 18,5 m do solo, que é a média da altura da base das copas das árvores das parcelas não-ardidas. A equação usou as seguintes variáveis: o percentil 80% da intensidade de retorno dos pontos e a percentagem de retornos acima de 18,5 m. O coeficiente de determinação desta foi R^2=0,93. O estado da floresta (ardida/não-ardida), expresso através de variáveis dummy, foi significativo para o modelo de regressão na equação.

Este trabalho mostrou que é possível realizar a estimativa da biomassa de áreas afetadas por fogos utilizando dados de deteção remota. A abordagem baseada em dados LiDAR permite que se faça a recolha dos dados de maneira mais prática do que os métodos de inventário convencionais, os quais exigem muito tempo e recursos para a sua execução.

Acknowledgements

I would like to express my special thanks of gratitude to my two advisors Professora Ana Paula Soares Marques de Carvalho, Professor João Manuel das Neves Silva and João Gomes Mota from Albatroz Engenharia who gave me the opportunity to research in this topic and continuously supported my study and research. Without the knowledge, equipment and help of João Gomes Mota and his company Albatroz Engenharia this thesis would not have been feasible.

Besides my advisors, I would like to formulate my deepest appreciation to Diogo Cosenza for the persistent help and the guidance throughout the whole research. He provided patient advice and help while preparing and analysing the point cloud data.

Contents

List of Figures

List of Equations

List of Tables

List of Abbreviations

3D	=	Three-Dimensional
AGB	=	Aboveground Biomass
ALS	=	Airborne Laser Scanning
CHM	=	Canopy Height Model
DNBR	=	Delta Normalized Burn Ratio
DTM	=	Digital Terrain Model
ESA	=	European Space Agency
FIREMON	=	Fire Effects Monitoring and Inventory System
GPS	=	Global Positioning System
ICNF	=	Instituto da Conservação da Natureza e das Florestas
LiDAR	=	Light Detection and Ranging
MNL	=	Mata Nacional de Leiria
MSI	=	Multi Spectral Instrument
MU	=	Management Unit
NBR	=	Normalized Burnt Ratio
NDVI	=	Normalized Difference Vegetation Index
NH	=	Normalized Height
NIR	=	Near-Infra-Red
OLS	=	Ordinary Least Square
RE	=	Red Edge
RMSE	=	Root Mean Square Error
SLAM	=	Simultaneous Localization and Mapping
SPOT	=	Satellite Pour l'Observation de la Terre
SWIR	=	Short Wave Infra-Red
UAV	=	Unmanned Aerial Vehicle
VIF	=	Variance Inflation Factor

1. Introduction

The tremendous impacts of forests fires that occurred in Portugal in 2017 are alarming. In this special case, Portugal's forests have not been spared and many areas in different locations were victims due to wildfires. Portugal's fires have burnt around 442.418 hectares of forest in the year 2017 (ICNF, 2019), 52 times the size of Lisbon and representing nearly 60 percent of the total area burnt in the entire European Union in 2017 (RUS-Copernicus, 2017).

Forest fires are a problematic and recurring issue not only in Mediterranean ecosystems, but worldwide (Fernández-Manso et al., 2016). Wildfires commonly burn extensive areas in forests and rangelands, which are important to society, wildlife, and the ecosystem in general (Morgan et al., 2014). Despite the extensive efforts to prevent, suppress, and mitigate wildfires, they continue to cause damage to wildlife and property. These damages include direct losses such as deaths, injuries, and structural damage along with business interruption, utility loss, and ecosystem impacts.

Moreover, wildfires frequently move into communities and burn buildings and infrastructures. On the other side of this topic, wildfires are naturally occurring and they play an important role in the life of a wildland area (Stein et al., 2013), but for planted forests that have an industrial purpose, forest fires can be problematic. Many of the environmental impacts are naturally recovered as the wildland area returns to its pre-fire state (Stein et al., 2013). These impacts do have real costs in the immediate aftermath of a fire and their effects can be exacerbated by human activity. Trying to completely avoid forest fires has a negative effect. By not having regular sweeps of fire through forested areas, the underbrush can grow to a point where the overabundance of fuel results in far more damaging fires (Thomas et al., 2017).

Measuring the magnitude of the fire damage in forests using remote sensing, could be important to plan post-fire recovery management and to quantify the losses of carbon stock (Chu and Guo, 2013). To find solutions after the fires, burned areas need to be evaluated individually. Due to the extensive areas affected by wildfires, it is hard to manage the post recovery actions from the ground only. The possibility of identifying and categorizing burned forests in different fire severity classes with the help of satellites or UAVs, where data is able to provide operational techniques that can be applied to large areas (Fraser et al., 2017).

To identify and categorize the consequences, the term fire severity was born (Keeley, 2009), with the need to provide a description of how fire intensity affected ecosystems, particularly following wildfires where direct information on fire intensity was absent and effects are often quite variable within and between different ecosystems. Most studies, that have attempted to measure fire severity, have had a common basis that centres on the loss of biomass of organic

matter, both aboveground and belowground. Aboveground metrics such as crown volume scorch (used in forests) or twig diameter remaining on terminal branches (used in forests and shrublands) are indicators of biomass loss (Keeley, 2009).

Remote sensing studies have found a good correlation between satellite imagery and fire severity estimates based on biomass loss (Keeley, 2009). LiDAR is an active remote sensing technology that is capable of capturing the three-dimensional (3D) structure of vegetation at high resolutions (both vertical and horizontal) and therefore it is now also being integrated into the studies of fire severity measurements (Angelo et al., 2010).

Over the last decades, remote sensing techniques have proven their usefulness to accurately estimate fire-affected areas and fire severity (Chuvieco, 2008). In this context, the Europe's Copernicus environmental monitoring programme Sentinel-2 gives continuity to the multispectral high-resolution optical observations over global terrestrial surfaces provided by the European Space Agency (ESA) through the Satellite for observation of Earth (SPOT) series of satellites (Fernández-Manso et al., 2016).

Fires consume vegetation, alter soil moisture and leave bare soil. The chlorophyll loss lead to changes in the visible, the Red-Edge (RE) and the Near-Infra-Red (NIR) wave-lengths (Escuin, Navarro, and Fernández, 2008) regarding leaves and branches. Most studies involving fire severity and remotely sensed data are based on Red, NIR and Shortwave Infra-Red (SWIR) spectral regions (Chuvieco, 2008). Chuvieco et al. (2002) stated that standard indices based on red and NIR bands (as Normalized Difference Vegetation Index, NDVI) increase its correlation to burn severity when using the upper part of the red band (RE). Korets et al., (2010) showed that RE based indices (indicators of chlorophyll content) were useful for quantifying and mapping forest damage due to fires in Siberia. The Multi Spectral Instrument (MSI) onboard Sentinel-2A records data in the vegetation RE spectral domain that is one of the best remote sensing-based descriptors of chlorophyll content (Fernández-Manso et al., 2016), providing an opportunity to assess red-edge spectral indices for burn severity discrimination. The mapping and analysis of areas affected by fire is not only important to assess the damage done physical and ecologically, but it also provides information on the right management activities after the fire to build recovery plans. There are different ways to determine the severity, one with data taken through fieldwork at the plot level or to do it with remotely sensed data (Cocke, 2005).

The delta normalized burn ratio (DNBR) is widely used to map post-fire effects from multispectral satellite imagery, but has not been rigorously validated across the great diversity in vegetation types. These data typically quantify spectral change between pre- and post-fire satellite images (Parks et al., 2014). The importance of these DNBR maps to fire rehabilitation

crews highlights the need for continued assessment of alternative remote sensing approaches (Smith et al., 2007).

The increasing acquisition frequency of airborne LiDAR data over relatively large areas offers a potential alternative mode of measuring fire-induced ecological change and calibrating reflectance-based spectral indices, such as DNBR, to improve the models that use index-based products. It has been well demonstrated, in the remote sensing literature, that the discrete-return LiDAR collected at high spatial resolution can accurately derive measures for the forest mean height or individual tree attributes, and provide three-dimensional canopy height and density metrics describing the vertical distribution of canopy material, aerodynamic roughness (Hudak, et al., 2009; Lefsky et al., 2002; Smith et al., 2007) and gap size (Hudak et al., 2009; Kane et al. 2013). When used with field data, LiDAR returns can also be used to predict forest attributes/variables/characteristics/measures such as basal area, volume, biomass, and leaf area (García et al. 2010; Hudak et al., 2009; Lefsky et al., 2002). LiDAR has been successfully used to quantify the effects of insect outbreaks in forests (Bater et al. 2010; Bright et al., 2012), pre-fire fuel loading (Andersen et al., 2005; García et al. 2011; Riaño et al. 2003; Seielstad and Queen 2003), and structural measurements of the post-fire environment (Bishop et al. 2014; Kane et al., 2013; Kwak et al. 2010; Wulder et al. 2009).

Airborne and satellite LiDAR measurements have allowed the development of novel techniques to accurately quantify the vertical and horizontal structures and the aboveground biomass (AGB) over a wide variety of forest ecosystems (Garcia et al., 2017). As most LiDAR data are currently acquired from airborne platforms, the data are often limited in terms of spatial and temporal coverage. Integration of airborne LiDAR with optical or Radar satellite observations provides a convenient alternative to overcome the shortcomings of LiDAR data availability, allowing for more accurate representation of the fuel load and the biomass dynamics, thus improving fire severity estimates. With airborne LiDAR, data as pre- and post-fire Canopy Height Models (CHM) can be related to fire severity (Alonzo et al., 2017).

LiDAR measures distances between a sensor and objects, based on the time lags between transmitting light amplification by stimulated emission of radiation (laser) beams from the sensor and receiving signals reflected from the illuminated objects (Chen, 2013). The distances derived from LiDAR, combined with the position of the sensor and the direction of the laser beam, uniquely determine the 3D coordinates of the objects illuminated. The errors of 3D coordinates vary with a myriad of factors, such as laser range sampling interval, global positioning system (GPS) positioning, inertial measurement unit, flying altitude, and surface reflectivity. But, in general, the vertical precision of position is on the order of decimetres for airborne and satellite LiDAR (Zwally et al. 2002; Chen, 2010). LiDAR remote sensing systems can be distinguished based on the way in which returned signals are recorded (discrete return

or waveform), scanning patterns (profiling or scanning), platforms (airborne, spaceborne or ground based), and footprint sizes (small-footprint: ~1 m or smaller, medium-footprint: ~10–30 m, or large-footprint: ~50 m or larger) (Lu et al., 2012). The most common configurations of LiDAR systems are airborne small-footprint discrete-return scanning LiDAR, airborne small-footprint discrete-return pro-filing LiDAR, airborne medium-footprint waveform LiDAR, and satellite large-footprint waveform systems. Ground-based systems and airborne small-footprint waveform systems are also emerging (Chen, 2013). Finally, with a more advancing payload on small UAV's (wings, multi-copter), which can operate at a much lower altitude compared to satellite and airborne plane acquisition, the scans get more detailed and therefore give more insight, in this example on the biomass loss due to fire.

Small-footprint LiDAR systems have proven to successfully correlate to AGB estimates in boreal and temperate forests (Kronseder et al., 2012). The remote sensing–based approach is appealing because it can provide spatially explicit estimates of the actual biomass at each pixel location, instead of only the average/total biomass within a given inventory unit (such as county, state, and country) (Jenkins et al., 2001).

The main goal of this thesis is to analyse the use of LiDAR techniques to quantify losses of biomass due to fire. To achieve that, MNL was chosen, because it was affected by the fire in October of 2017. The fire severity was estimated by pre- and post-fire images from satellites like Sentinel-2, which supported the selection of the plots to carry out the study. Because MNL has areas with low and medium to high fire severity, we chose a management unit (MU), which has both severity classes. Both burned and unburned areas were scanned by flying an UAV with LiDAR sensors. We intended to test whether there were significant differences between the AGB of both areas and, if so, to quantify the loss of AGB associated with fire. For the estimation of the AGB also a dummy variable (burned/unburned) is going to be used to find out if the state of the forest has an impact on the linear regression model.

2. Mata Nacional de Leiria – History

The National Forest of Leiria (Mata Nacional de Leiria – MNL) is an example of fixation of soil and land due to what would be lost by continuous dune spreading (Pinto, 1939). To implement norms for fixing the sand dunes for the conservation a former king of Portugal already setup management plans. The maritime pine (*Pinus pinaster* Aiton) is fixing the sands to stop the advancing dune growth towards the inland and the burying of agricultural lands. The MNL planning has always aimed at preserving this ecosystem created over the years. Any more "daring" intervention in the MNL, destroying or altering its vegetation cover (*maritime pine*), would destabilize this ecosystem, causing the disappearance of the soil, which is being formed on the wind sands, exposing agricultural crops from the periphery to the advancement of sands and sea winds (André and Cordeiro, 2016). Therefore, it is important to protect this forest and in case of natural or human disturbances (windthrows, forest fires, pests, and diseases) trying to find the best possible management options to keep the ecosystem in a balance.

The MNL, located at Marinha Grande county, represents Portugal first planned area of maritime pine (Marques, 2010). This species is one of the main species in the national forest landscape and it is of great economic and social importance, especially in Central and Northern regions. The studied area has a humid temperate climate (mesothermal), with a dry, long and cool summer, according to Köppen classification. The geological substratum is largely dominated by Quaternary formations, which include mainly sand dunes and Pliocene sediments consisting of dunes and sand dunes. The relief is plain/flat to undulating, depending on the expression of the dunes, which form three main strands which roughly follow the direction of the coast. In addition to the pine, the shrubby and herbaceous species more abundant are the heather (*Calluna vulgaris* (L.) Hull), Yellow Rock Rose (*Halimium calycinum* (L.) K. Koch), Sage leaf rock rose (*Cistus salvifolius* L.), Braken (*Pteridium aquilinum* (L.) Kuhn), and Gorse (*Ulex europaeus s*ubsp. *latebracteatus* L.) (Marques, 2010).

3. Data and Methods

3.1 Study area

MNL is located on the coast of Portugal, approximately, 140 kilometres north of Lisbon (39°46'18.30''N; 8°58'05.35'' W) and covers around 11,080 ha (Figure 1). This number corresponds to about 60% of the area of the municipality of Marinha Grande (Alcarva, 2011). The site is covered mainly by pure stands of maritime pine with different age classes. MNL is divided in 342 rectangular management units with, approximately, 35 ha each. It has a maximum width of 8,394 m and a maximum length of 18,549 m.

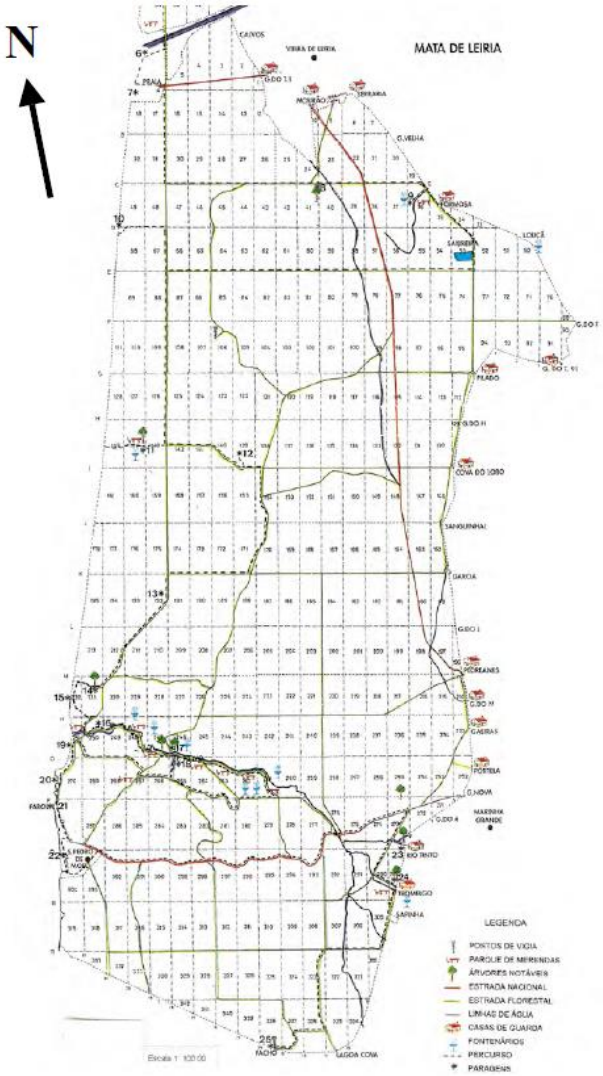

Figure 1: Plan of the management units in MNL

3.2 Site selection

With the goal of distinguishing differences in the LiDAR metrics between burned and unburned areas of the forest, we localized spots in the forest where both burned and unburned occurred close to each other, in the same management unit. While the fire on the 15th and 16th October 2017 ran over the MNL with a high speed, there were still isolated parts that were not burned. With the guidance of the fire severity map and the requirements for the UAV flights, the management unit 220 (Figure 2) was chosen.

Two areas with the size of 60x120 m (7200 m²), one part was unburned and one was burned, were established for the field inventory and the UAV flights (Figure 2, Area 1 and Area 2). In each of these areas, two inventory plots of 1600 m² of area (40 m x 40 m) were installed:

- P1B and P2B, burned plots with moderate to high fire severity, and
- P1U and P2U, unburned or burned plots with low fire severity.

The area of each plot – 1600 m^2 – corresponds to the area of 4 pixels of Sentinel-2 images.

To increase the number of degrees of freedom of the regression equations, each plot was subdivided into four subplots, with a size of 20 x 20 m (400 m²) (Figure 2).

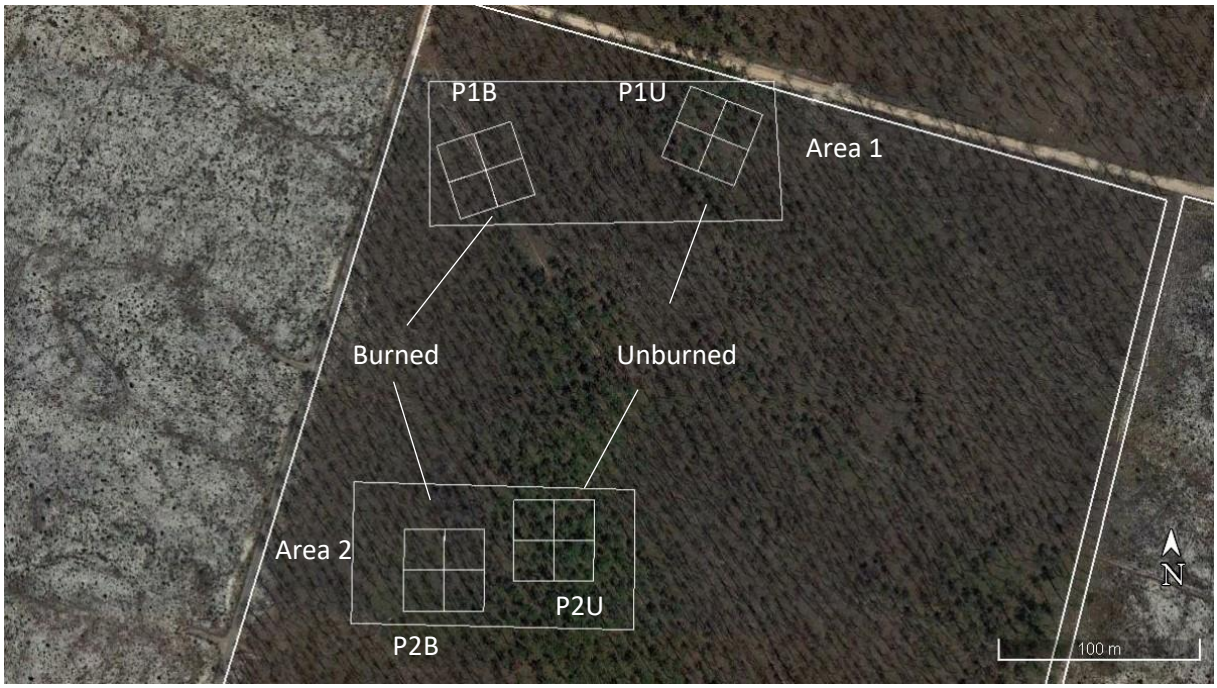

Figure 2: Map of management unit 220 with the two areas for the UAV flights and the 16 subplots

3.3 Field inventory and methods

In May-June 2018, field inventory was carried out on the four square plots (P1B, P1U, P2B, P2U, Figure 2). Most of the trees had a straight stem, only few of the trees in the field plot had forked stems (Figure 3). At the end, a total of 148 maritime pine trees were measured – 75 in unburnt plots (P1U+P2U) and 73 in burnt plots (P1B+P2B). The total height and the diameter at 1,30 m height (dbh) were measured in all trees. In the unburnt plots, the height of the crown base of all trees was measured. Tree coordinates were also registered, with a sub-metric precision GPS (Trimble, with a GPS ProXH receiver)

Table 1 presents the main characteristics of the 4 plots. Plots located in the same area (P1U and P1B in Area 1, P2U and P2B in Area 2) are very similar, as intended. Area 2 has a higher site index than Area 1 (in this case, site index is the dominant height at 50 years and it is a measure of productivity), associated to higher number of trees per hectare, quadratic mean dbh, and stand basal area.

Table 1: Main characteristics of the 4 plots used in this study

	P1U	P1B	P2U	P2B
N (ha^{-1})	225	225	244	231
t (yrs)	68	68	68	68
hdom (m)	24,6	24,3	29,1	28,2
hm (m)	24,1	24,1	27,9	27,4
dg (cm)	36,4	35,8	38,7	38,2
G (m^2/ha)	23,5	22,6	28,6	26,5

where N is the number of trees per hectare; t is the stand age; hdom is the dominant height defined as the mean height of the 100 largest trees per hectare; hm is the mean height; dg is the quadratic mean dbh, and G is the stand basal area; P1U and P2U are the unburned plots, and P1B and P2B are the burnt plots.

Figure 3: Left: The burned forest, Right: Field data collection

Data from inventory were used to estimate tree AGB (Formulas 1 - 6) (Faias, 2009), that was expressed as the sum of the tree biomass components: wood (w), bark (b), branches (br), and leaves (l). The stand AGB was defined as the sum of the aboveground biomass (Formula 6) of all trees in each plot expanded for the hectare. For the unburned and burned plots were used total aboveground biomass and aboveground biomass without the needles component, respectively (Figure 4).

ύ ύ سی πἴππφςτω ὀيٰ٢يٍ٦٠٠١ ῼ٥ٰ٦يٍ٣٧٢٣ ῼيٰ٧٢٣١٧٥ (1)

ύ ῴ سی πἴππψ ὀيٰ١٣٦١يٍ١ ῼ٠ٰ٦يٍ٥٧٦١ (2)

ύ ῴ ὶ سی πἴππσσχς ῼ٠ٰ٦يٍ٥٣٤٣ (3)

ύ ἀ سی πἴπφρψτσ ῼ٥ٰ٤٥٦٧٥٤ ثـ/ز ٩يٰ٣٥٢٥١ (4)

ύ ί سی ύ ύ ط ύ ῴ (5)

ύ ῴ سی ύ ύ ط ύ ῴ ط ύ ῴ ὶ ط ύ ἀ (6)

ww, wood biomass (kg); wb, bark biomass (kg); wbr, branches biomass (kg); wl, leaves biomass (kg); ws, stem biomass (kg); wa, aboveground biomass (kg); t, age (yrs); d, diameter at 1,30 m height (cm); h, total height (m)

Figure 4: Left side: unburnt or low fire severity burnt area; right side: high fire severity burnt area. These photos are from a MU next to the one used in this work (credits: P. Soares)

3.4 Sentinel-2 data and fire severity

With remote sensing, the standard procedure to estimate fire severity is to use two satellite images (one pre-fire and post-fire), to derive a spectral index related with the effects of fire (e.g. Normalized Burnt Ratio - NBR) and to compute the temporal difference (pre- minus post-fire) of the index (e.g. DNBR). Satellite imagery used in this study was chosen such that pre- and post-fire dates were as close to the dates of the fire as possible, to reduce all influence that is not connected to the fire. All pre- and post-fire images were acquired with cloud and smoke-free sight on the plot (Miller and Thode, 2007).

The NBR (Formula 7) was designed to highlight burned areas and estimate fire severity. The formula is similar to NDVI, except that it uses NIR and SWIR wavelengths, instead of the NIR and the visible radiation (Lutes et al., 2006).

$$\text{Ŭ ŏ'Y سي } \frac{\text{ئآبئ٩ ئآ إ}}{\text{ئآبئ٨ ئآ إ}} \qquad (7)$$

Unburned healthy vegetation has very high NIR reflectance and low reflectance in the shortwave infrared portion of the spectrum. Recently burned areas have relatively low reflectance in the NIR and high reflectance in the shortwave infrared band. A high NBR value generally indicates healthy vegetation while a low value indicates bare ground and recently burned areas (Humboldt State Geospatial Online, 2014).

Higher DNBR (Formula 8) indicate more severe fire damage. Areas with negative DNBR values may indicate vegetation re-growth following a fire.

$$\text{\$. " 2 سي ŭ ì'Ω'ΩìΩŭ ŏ'Y طي ŭ ɛ í ò'ΩìΩŭ ŏ'Y} \qquad (8)$$

The meaning of the DNBR values can vary from image to image, and for best results interpretation in specific instances should always be based on field assessment. These guidelines are then used to create a thematic burn severity layer depicting severity as low, moderate and high (Humboldt State Geospatial Online, 2014).

For the categorization of the different levels of fire severity with the Landsat-2 data, at least, three levels should be stablished (low, medium and high). In this study, seven levels were defined, using Sentinel-2 images (Table 2).

Table 2: Fire Severity classification

DNBR	Fire Severity
< -0,25	High post-fire regrowth
-0,25 to -0,1	Low post-fire regrowth
-0,1 to +0,1	Unburned
0,1 to 0,27	Low-severity burn
0,27 to 0,44	Moderate-low severity burn
0,44 to 0,66	Moderate-high severity burn
> 0,66	High-severity burn

3.5 LiDAR data acquisition and processing

The LiDAR data were acquired with a VLP-16 Velodyne LiDAR PUCK™ mounted on a multicopter in early May/June 2018 from an average altitude of 60 m above the ground level. In this flight campaign the LiDAR system was configured to record up to two returns per laser pulse, i.e., first and last. The reported horizontal and vertical accuracies are ±3 cm, respectively, according to the technical information of the producer. The flight path was designed to have 50% swath overlap to cover all the area with a necessary number of scans. The flightpaths were oriented according to a lawnmower pattern, flying from north to south across the plots (Figures 5-6). The GPS precision of the flying drone was not sufficient to match different scan lines into a 100% matching image. Therefore, the scan angle of each flight line was reduced to ±35° (nadir) to not let the overlap/double vison of shapes disturb the whole point cloud.

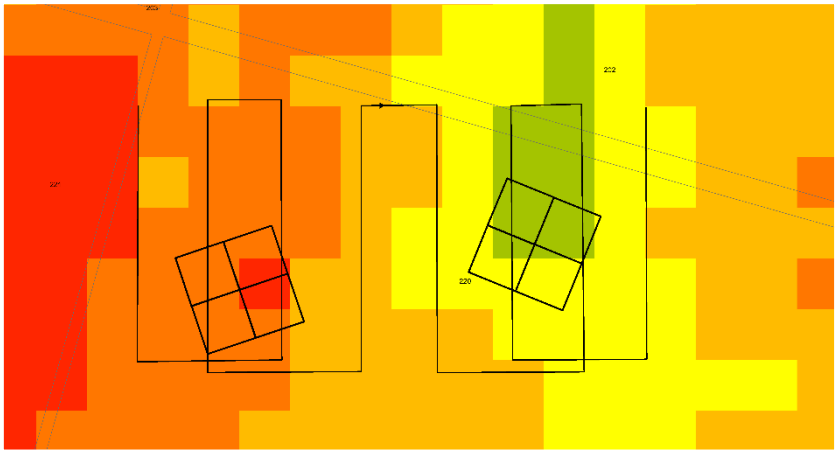

Figure 5: Lawn moaner-pattern of the UAV in Area1- P1U and P1B plots

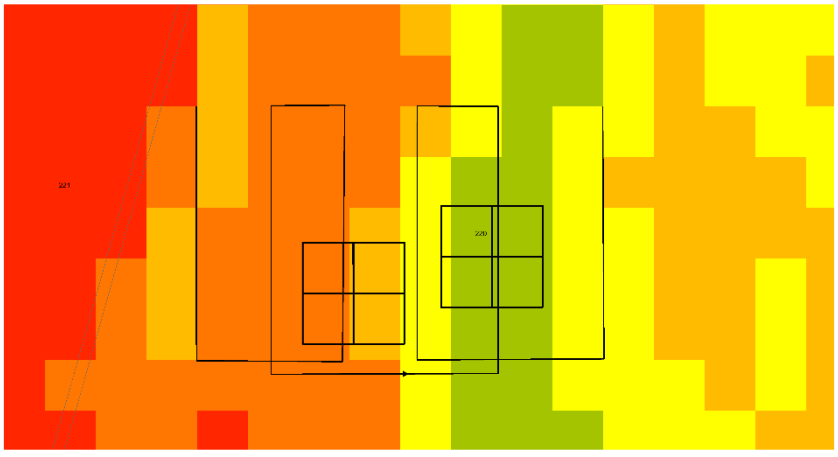

Figure 6: Lawn moaner-pattern of the UAV in Area2 – P2U and P2B plots

In Table 3, technical details of the laser scanner used are described.

Table 3: Technical details of the laser scanner/Laser system parameters for LiDAR data collection

Parameter	Value
Model	VLP-16 Velodyne LiDAR PUCK™
Channels	16
Measurement Range	Up to 100 m
Accuracy	±3 cm (Typical)
Returns	Single and Dual Returns (Strongest, Last)
Field of View (Vertical)	+15,0 to -15,0 (30)
Angular Resolution (Vertical)	2,0
Field of View (Horizontal)	360
Angular Resolution (Horizontal/Azimuth)	0,1 – 0,4
Rotation Rate	5 Hz – 20 Hz
Point Density [Points/m^2]	±150
Pulse duration [ns] (Duration)	6
Repetition Rate [KHz] (repetition)	21,7
Measurement Rate [pts/s]	~300.000
Power consumption [W]	8
Net weight [kg]	0,83

Regression models were used to develop equations to relate LiDAR-derived parameters with stand AGB.

For processing the point clouds, the FUSION software V.3.4.2 (McGaughey, 2018) was used for filtering and interpolating data and generating:

- the Digital Terrain Model (DTM),
- the Canopy Height Model (CHM), and
- the Normalized Height (NH) of the Airborne Laser Scanning (ALS) point cloud,

which were necessary as input data for generating the cloud metrics. These were used to fit equations to estimate stand AGB.

The FUSION software v3.8 (McGaughey, 2018) was run on R environment (RStudio Team, 2016) and the lidR package (Roussel, 2019) was applied for LiDAR data manipulation. The following processing steps were carried out:

1. The acquired point clouds were cut, using the PolyClipData tool, into the size that contain all the subplots, to save work doing the further tooling in a big cloud and then in the end separating into the smaller parcels.

2. Outliers were removed using the FilterData tool, considering a window size of 35m and a factor of 2.5. These parameters were selected after several tests to be proven good and giving appropriate results to clean the cloud from unnecessary points.

3. The GroundFilter tool, which implements a filtering algorithm based on linear prediction, was used to extract ground returns from all the ALS points with a cell size of 1 m. The following parameters were also used to extract the bare earth points: gparam=-2,0; wparam=2,5; and using 5 interactions.

4. A DTM grid, with 1 m cell size, was created with the GridSurfaceCreate tool, which estimates the elevation of each grid cell from the lowest elevation of all points within the cell; if the cell does not contain any points, it is filled by interpolation from the neighbouring cells.

5. Following, the ClipData tool was used to obtain the normalized heights by subtraction of the ellipsoidal height of the DTM from the ellipsoidal height of each ALS return (Magdon et al., 2018).

6. Finally, the extraction of metric from the point cloud was carried out by using the CloundMetrics command. The CloudMetrics command generates a csv (.txt) file with 102 metric key values about the properties of the point cloud.

3.6 Modelling approach

After extracting the cloud metrics values for each of the subplots with the Fusion software package, the values were used to fit stand AGB equations.

An exhaustive search was applied to select the best independent variables for the equations. An all-possible regression algorithm was used to select the best model with three predictors, out of a large set of variables. Multiple linear models fitted through ordinary least square (OLS) regression were applied, where the response variable has been square rooted to avoid problems of heteroscedasticity (Sheridan et al., 2015). The presence of collinearity in the models was analysed through the values of the variance inflation factors (VIF), using the value 10 as the upper limit (Steinhorst and Myers, 1988).

The selection of the best model was based on measures of prediction ability, and the root mean square error (RMSE, Formula 9) was used.

$$RMSE\ (\%) = 100 \times \frac{1}{\bar{y}} \sqrt{\frac{\sum_{i=1}^{n}(y_i-\hat{y}_i)^2}{n}} \qquad (9)$$

Where n is the number of plots (n=16); y_i and $\hat{y}_i$ are the observed and estimated stand AGB (t/ha) for the subplots i=1…16, respectively; $\bar{y}$ is the observed mean stand AGB.

A dummy variable related to the plot status (burned/unburned) was added to the best model and it was fitted through OLS. All the fitted parameters were tested (t-test, α=5%) and the non-significant ones were removed, and the model was refitted.

4 Results

4.1 Fire severity map

In this study, Sentinel 2A and 2B images (acquired on 15th and 17th October 2017) were used to derive the DNBR. The fire in MNL occurred on the 17th October and lasted only one day. The derived DNBR values ranged from unburned to high severity burned areas (Figure 10). The distance from unburned to high severity patches is in some cases smaller than 100 meters, revealing the spatial variability of fire severity. When analysing the severity map in the field, different effects were observed. First, the small slopes and hills inside the forest had an effect on fire severity. In the smaller valley-like areas, the severity was not as high as on the hilly areas. Because the fire was burning the area in a short time (two days), in the large majority of the area only stems and crowns of the trees have been affected. This was clearly visible while distinguishing the different severity levels. The stems of the trees of the burned areas were completely black, nearly to crown height. The crowns of most of these trees were brown because they dried out due to fire. In the areas classified as unburned on the fire severity map, no traces of fire, neither on the stems, nor on the crowns were observed in the field.

In the picture (Figure 7 and also Figure 4), the separation between lower and higher severity is visible. The right side of the picture has no visible intact crowns, all needles were either burnt completely or dried and fell off. Compared to the right bottom where the top crowns of the trees are still alive.

Figure 7: Border between unburned (left) and burned areas (right)

With Formula 8 the DNBR image was produced, by subtracting the pre- (Figure 8) from the post-fire (Figure 9) image. In Figure 10 there are mentionable differences. The dark red coloured plots are mostly young stands or only areas with shrub vegetation. The parts with dark and light green parts on the right side of the image are the unburned parts, where the forest ends and the nearby city starts. Also, some green lines cross the burned areas, which are sometimes caused by rivers that flow through MNL.

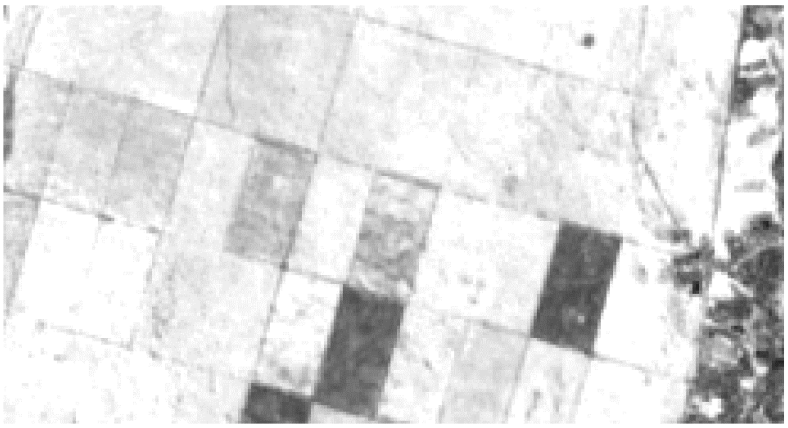

Figure 8: Pre-NBR image taken on the 15th of October

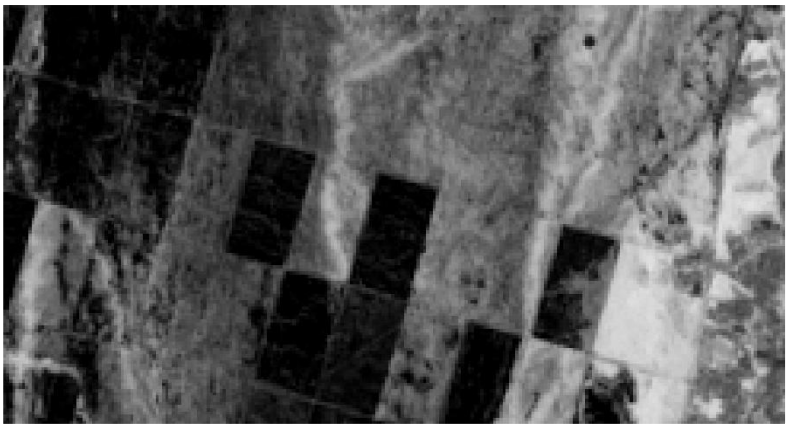

Figure 9: Post-NBR image taken on the 17th of October

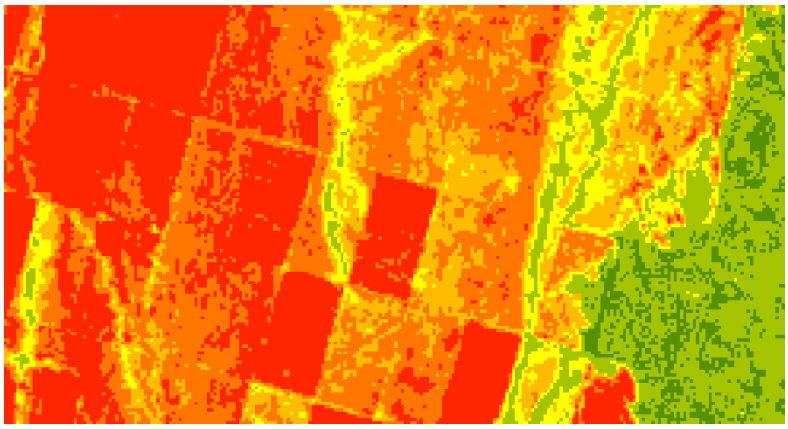

Figure 10: DNBR map of the study area

The classification was divided into seven categories (Table 2), starting with a high regrowth of vegetation and ending with the highest severity possible.

In Figure 11, the four forest inventory plots are visible, and the severity of the fire is classified. The division of the border between the more fire severe areas and the less harmed areas is clear. For this work two of each, unburned and burned, have been used and selected. The subplots for each of the plots were numerated, following the Figure 12.

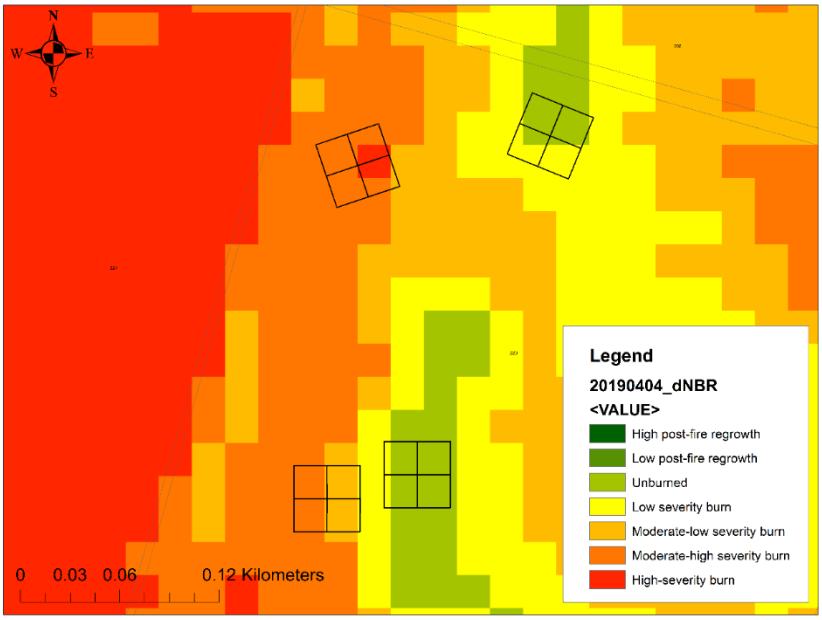

Figure 11: Final DNBR image of the study area with the field inventory plots

The first number is the general division between the first drone flight areas, the second position stands for either burned (B) or unburned (U) and the last position gives the number of the subplot.

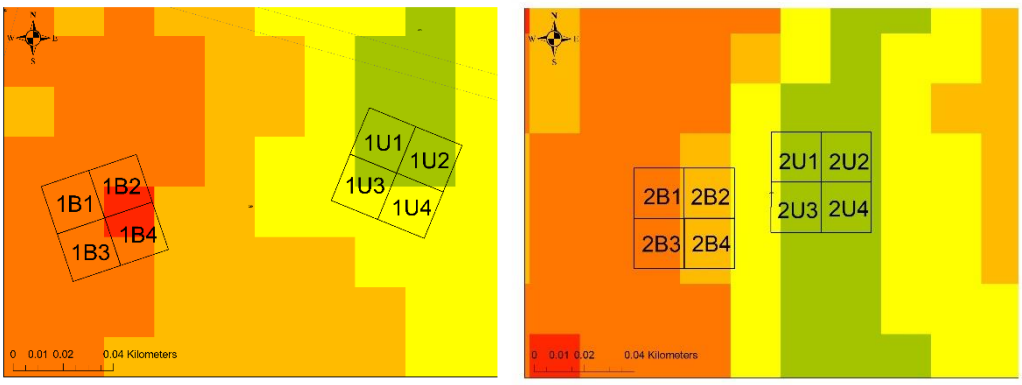

Figure 12: Division of the four plots into the 16 subplots

4.2 LiDAR point clouds

The cleaned and normalized clouds, taken from one flight, are displayed in Figures 13, 14, and 15, and they have some noticeable specific details.

The more severe burned areas, visible on the left side of the scans, have a lower point number in the bottom part of the scans. It is expected that the laser beams could penetrate more in regions where the canopies have less needles, so that more points would be present in the bottom of the cloud. In the side view of the first scanned area, on the left-side, the high severity and on the right-side unburned area, it is noticeable that the trunks were almost completely missing. However, as presented in the Figure 16, the trunks on the high severity plots were burnt till a height of approximately sixteen meters, so that the stems till the crown were fully black, probably causing the absorption of the laser light.

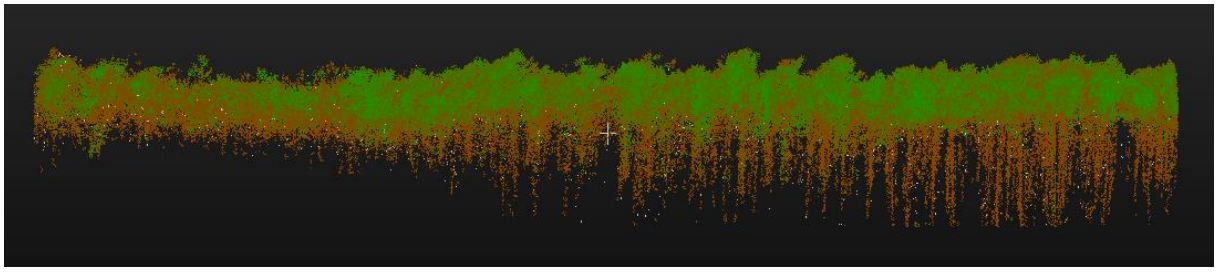

Figure 13: Side view of a cleaned and normalized point cloud without ground

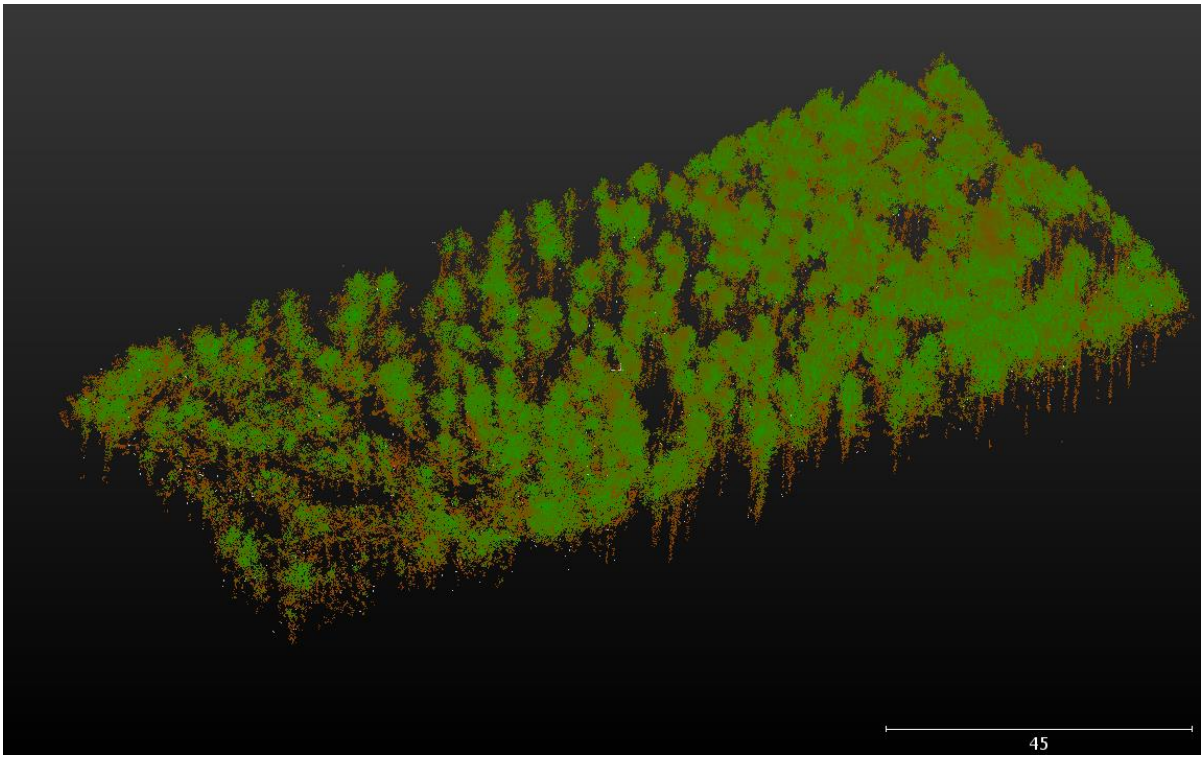

Figure 14: ISO view of a cleaned and normalized point cloud without ground

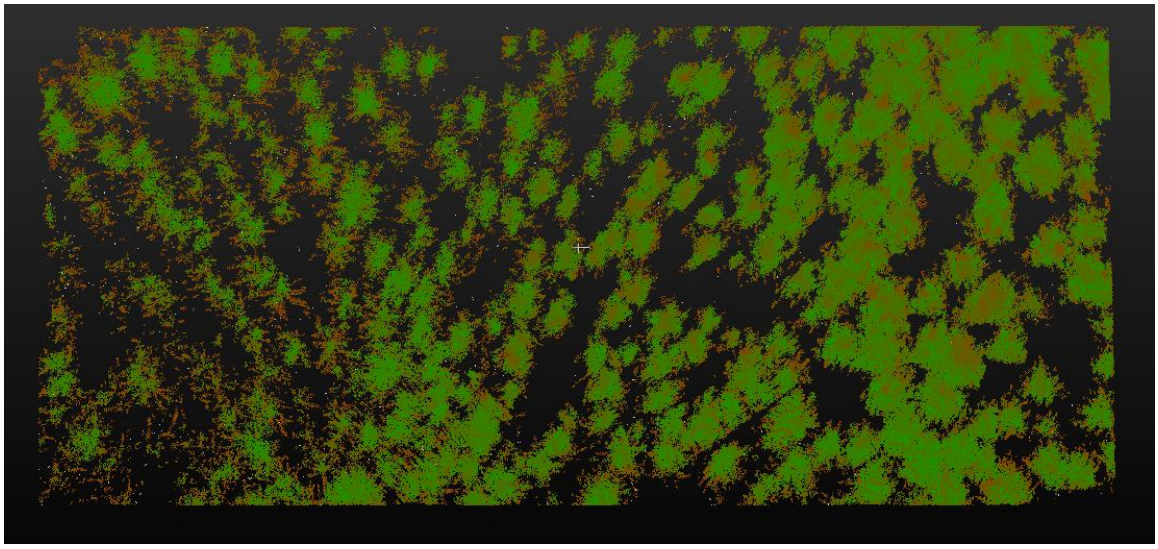

Figure 15: Nadir view of a cleaned and normalized point cloud without ground

Figure 16: Picture of the burned (moderate-high severity) area with half burned (low severity) trunks of trees

From the LiDAR data processing, as mentioned in chapter 3.5, resulted a set of 102 metrics that characterize each subplot point cloud (see Appendix). Metrics were extracted from points laid above 1 meter from the ground.

4.3 Estimates of aboveground Biomass using data from inventory

In all the plots, the stand AGB ranges from 105 to 186 t/ha, approximately, except the subplot 2U4 (Table 4), which has a larger number of higher trees. This subplot has the highest mean tree aboveground biomass with 921,2 kg.

Table 4: Characterization of the 16 subplots

Plot	Subplot	Wa (t/ha)	wa (kg)	wam (kg)	hm (m)	ntrees
P1B	1B1	124,99	4999,59	555,5	25,3	9
	1B2	170,26	6810,21	619,1	24,0	11
	1B3	133,93	5357,11	595,2	23,8	9
	1B4	105,14	4205,43	600,8	23,3	7
P1U	1U1	178,89	7155,63	596,3	23,6	12
	1U2	135,74	5429,67	678,7	24,4	8
	1U3	136,25	5450,14	681,3	24,3	8
	1U4	128,91	5156,46	644,6	24,2	8
P2B	2B1	186,15	7446,08	744,6	27,7	10
	2B2	141,58	5663,31	707,9	27,0	8
	2B3	178,58	7143,23	793,7	27,3	9
	2B4	179,13	7165,19	716,5	27,3	10
P2U	2U1	161,23	6449,16	716,6	26,8	9
	2U2	146,78	5871,03	838,7	28,0	7
	2U3	148,77	5950,81	661,2	27,4	9
	2U4	322,41	12896,52	921,2	28,9	14

where Wa is the aboveground biomass (t/ha); wa is the subplot aboveground biomass (kg/400 m^2); wam is the mean tree biomass (kg); hm is the mean tree height (m); ntrees is the subplot number of trees.

4.4 Estimates of aboveground biomass using LiDAR metrics

The final selection of the aboveground biomass equation for maritime pine (Formula 10; Table 5) is a function of the highest point height value, the kurtosis of the point height values and the height correspondent to the 80th percentile of the point heights. The minimum, average and maximum values for these variables, at subplot level, are presented in the Appendix.

The final equation is:

$$\widehat{AGB} = -54.79637 - 0.43053\, HTmax + 0.20532\, HTkurt + 3.21581\, P80 + 57.87677\, Dum.U + 0.67376\, HTkurt \cdot Dum.U - 2.46241\, P80 \cdot Dum.U \qquad (10)$$

where $\widehat{AGB}$ is the predicted aboveground biomass (t/ha); *HTmax* is the maximum height (m); HTkurt is the kurtosis of the distribution of all return heights; P80 is the 80th percentile of height (m); $Dum.U$ is the dummy variable being 0 for burned plots and 1 for unburned plots. The variable *HTmax* was not tested in connection with the dummy variable, because the height of trees wouldn't change from burned to unburned plots.

Table 5: Statistical analysis of the results above 1 meter, including testing for fire effect through the incorporation of a dummy variable concerning the status (burnt vs unburnt)

Regressor variable	Coefficient	Standard dev.	t value	*p*-value
Intercept	-54,79637	13,99	-3,918	≤ 0,01
HTmax	-0,43053	0,10	-4,104	≤ 0,01
HTkurt	0,20532	0,06	3,366	≤ 0,01
P80	3,21581	0,59	5,463	≤ 0,01
Dum.U	57,87677	14,57	3,973	≤ 0,01
HTkurt: Dum.U	0,67376	0,12	5,802	≤ 0,01
P80: Dum.U	-2,46241	0,58	-4,219	≤ 0,01

The relation between AGB estimated with allometric equations and LiDAR variables is depicted in the Figure 17. It is possible to note a point standing out, which corresponds to subplot 2U4, previously described closer in chapter 4.3. It is not a statistical outlier since it matches to the regression line and the data behind it is not false or wrongly measured. It is a special characteristic of the subplot. Furthermore, the R^2 value of the equation is 0,94 and the adjusted R^2=0.89, showing a good accuracy of the model (Figure 17).

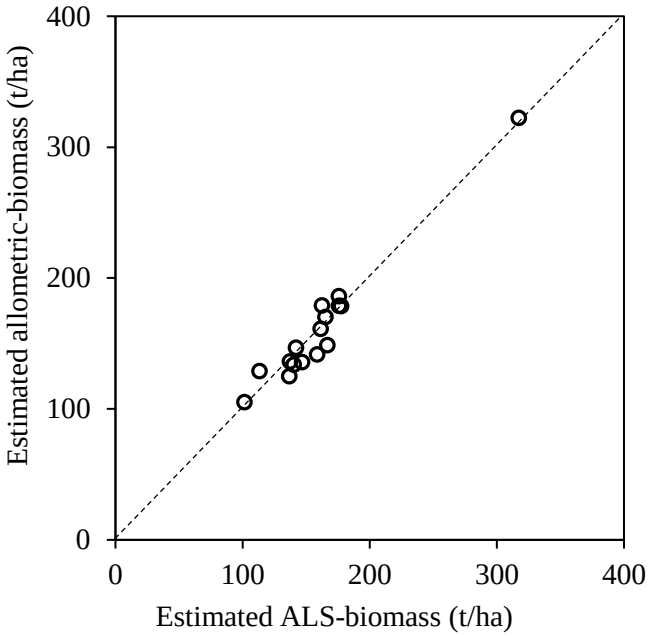

Figure 17: Comparison of estimated allometric-biomass and estimated ALS-biomass with the regression line (height threshold 1 m)

For Formula 10, the total AGB and the LiDAR metrics of one meter above ground level was used. It shows a good correlation and takes into account mostly metrics values, that are connected to tree height and tree crown characteristics (*HTmax*; HTkurt; P80).

Despite the small number of observations, the residues of the linear regression model (Figure 18) are well distributed with no atypical tendency of heteroscedasticity, which indicates a good behaviour of the linear model.

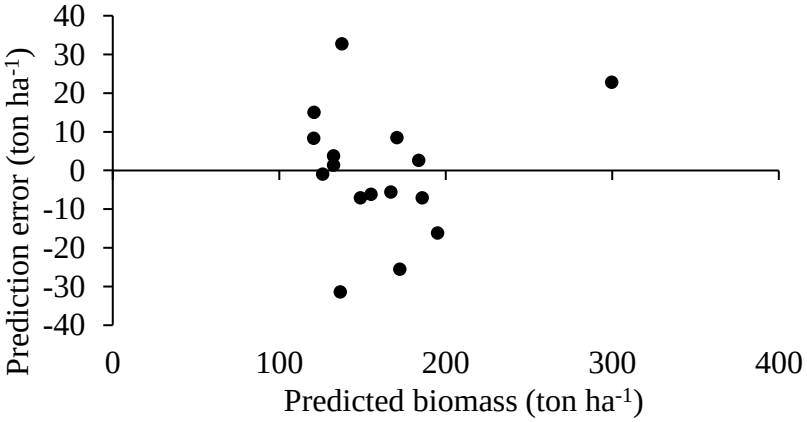

Figure 18: Distribution of the residuals of Formula 10

Based on the results of the first biomass estimation, another equation (Formula 11, Table 6) was fit. This one takes into account the full AGB, as in Formula 10, but only the LiDAR metrics above the height of 18.5 meter, which is the threshold of the average crown base height.

$$\overline{AGB} = 11{,}02175 + 1{,}34501 \cdot INTP75 - 1{,}34666 \cdot INTP80 + 0{,}12117 \cdot PercAAL + 15{,}02894 \cdot Dum.U - 1{,}00996 \cdot INTP80{:}Dum.U + 0{,}15765 \cdot PercAAL{:}Dum.U \quad (11)$$

where $\widehat{AGB}$ is the predicted aboveground biomass (t/ha); *INTP75* is the 75th percentile connected to the metrics intensity; *INTP80* is the 80th percentile connected to the metrics intensity; *PercAAL* is the percentage of all returns above the threshold of 18,5 meter; $Dum.U$ is the dummy variable being 0 for burned plots and 1 for unburned plots. The variable *INTP75* was not connected to the dummy variable for the equation, because it was not significant enough.

Table 6: Statistical analysis of the results above 18,5 meters, including testing for fire effect through the incorporation of a dummy variable concerning the status (burnt vs unburnt)

Regressor variable	Coefficient	Standard dev.	t value	*p*-value
(Intercept)	11,02175	4,75036	2,32	0,04547
INTP75	1,34501	0,37683	3,569	0,00603
INTP80	-1,34666	0,36412	-3,698	0,00493
PercAAL	0,12117	0,05126	2,364	0,04233
Dum.U	15,02894	6,53933	2,298	0,04714
INTP80:Dum.U	-1,00996	0,26374	-3,829	0,00403
PercAAL:Dum.U	0,15765	0,05873	2,684	0,02503

The R^2 value of the equation (Formula 11) is 0,93 and the adjusted R^2 equals 0.88, displayed in Figure 19. This model is closely as good as the previous showed model around Formula 10. The relationship between the estimated and the calculated AGB through the fitted equation (11) has a linear correlation, also with one point being more far away from the main group of points. Moreover, the variables used in this second equation show that the tree crowns alone give insight into the overall AGB and the status (burned/unburned) of the forest.

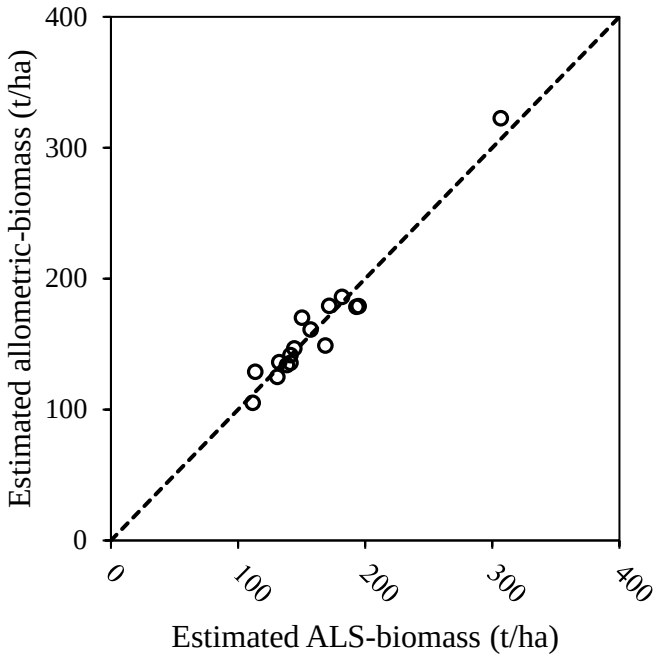

Figure 19: Graph comparing estimated allometric-biomass and estimated ALS-biomass with the regression line (height threshold 18,5 m)

Similar results for the distribution of the residues, compared to Formula 10 (Figure 18), were obtained for the second linear regression model (Formula 11, Figure 20). The graph shows no clear pattern in the distribution of points, which also indicates a good fit of the model.

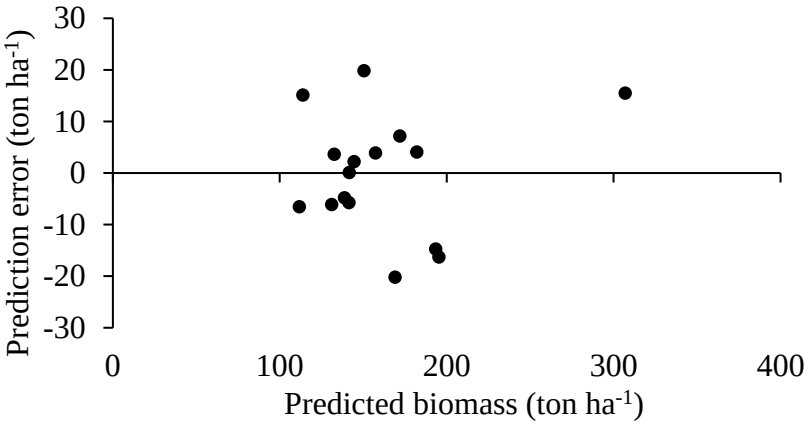

Figure 20: Distribution of the residuals of Formula 11

5 Discussion

In this study different data and methods were used and combined to analyse the effect of forest fires on the loss of biomass in the MNL. The results of the DNBR severity mapping of the affected area were precise and accurate to the scale that the Sentinel-2 imagery made it possible (1 pixel=400 m^2). The calculated severity map showed the status of the forest successfully, as proven through the FIREMON - Fire Effects Monitoring and Inventory System (Lutes et al., 2006). Since the fire was moving very fast through the MNL, it did not have an impact correlated with massive biomass loss; instead, it showed scorched stems and dried out crowns. The severity classification is based on NIR and SWIR reflectance of the crowns and it gave precise correlations, because the unburned areas still had healthy/green tree crowns (high NIR, low SWIR) and the burned/dried tree crowns (low NIR/, high SWIR) showed a reversed spectral pattern.

The following LiDAR scans with a UAV flying at low altitude (sixty meters aboveground) gave sufficient data for the following analysis. Also, mentionable differences between low and moderate burned areas were found as described in chapter 4.2. The missing reflectance characteristics of the burned stems were not foreseen, but the two models were derived, one with data using a height threshold 1 m and other with a height threshold 18.5 m, to gain insight in the impact of losing the laser data of the stems.

The estimated AGB values with the fitted regression model were accurate to a correlation of R^2=0,94. Even with the point cloud characteristics showed in chapter 4.2, that resulted in an absence of the trunks in the point cloud, the equation 10 shows results, which could be useful for further research. Additionally, also the second equation (Formula 11) had a good correlation with a R^2 value of 0,93. The residues of the two fitted linear regression models show no patterns and are well distributed, which states a good fit of model. By looking at the influence of the dummy variable on the models, both have one thing in common. When the dummy alone is used for unburned plots (1 = unburned, 0 = burned), it increases the intercept, resulting in a higher biomass value. For the equation 10 the variable *P80* connected to the dummy has a negative and *HTkurt*, also in connection with the dummy, has a positive influence on the slope of the model. In equation 11 there is a negative influence of *INTP80* and a positive effect of *PercAAL* on the slope connected with the dummy variable.

Comparable studies, done with a lower resolution of LiDAR scans, came to accuracies of determining the biomass based on scans with an R^2=0,88 (Popescu, 2007). These were done with an equation based on dbh and canopy height. Most studies and tests were done at an acquisition altitude of the point clouds higher than 60 meters and therefore have a much lower

point density per m². The studies of Lu et al (2012) come to results of an R^2 of 0,75–0,77 with a logarithmic transformed equation. A study done by Sato et al. (2016) came also to AGB estimations based on LiDAR metrics, that explain 69% of the total variance across forest types. The equation was based on these LIDAR metrics variables: mean of height, the third quartile of height, the tenth percentile of height, and the kurtosis of the distribution of all return heights (Sato et al., 2016), which are based on a research of Longo et al. (2016). Though the equation of Sato et al. (2016) was based on an exponential approach it still shows similarities, in the LiDAR metrics values used, to the equation built with this study. The most significant variables taken from the point cloud metrics to fit the equations are mostly height and tree crown connected. Nevertheless, it needs to be mentioned that it is not a simple task to compare the accuracies between different approaches to estimate biomass. Each work uses a particular approach to model the dataset and so to assess the model's accuracy.

By comparing the estimated-allometric biomass with the estimated ALS-biomass, good correlations were found in this study. With the dummy variable, the equation also considered the state of the forest (burned or unburned). As the dummy was significant, which gives stronger evidence that it is possible to distinct between the two states of the forest and calculate the corresponding/respective biomass.

6 Conclusions

The analysis of the fire severity through remote sensing techniques, like the DNBR calculated with pre- and post-images of the burned area, gave satisfying results. In this study, the DNBR classification was necessary to decide which sample areas to choose for the more detailed analysis of the burned and unburned areas. Nevertheless, this type of severity analysis showed medium high to low/unburned severity levels. The most obvious changes, also the most crucial, were that the understory shrubs got burned, the stems were nearly fully burned on the outside and the needles got dried out. These characteristics can be analysed with the DNBR technique. However, others like volume or biomass cannot.

In general, the fitting of the equation with the six variables compared to the field-measured biomass showed accurate results with a R^2 of 0.94 (Formula 10) and a R^2 of 0,93 (Formula 11). The first equation takes into account 4 different main key values. First the maximum height (*HTmax*) of the point cloud, which didn't change through the burned and unburned areas, but gives more predictability power to the equation. Secondly, the variable HTkurt, which gives insight in the probability distribution shape and the vertical distribution of the points. More important is the variable P80 that describes the 80th percentile of the point cloud and is connected to the crowns of the trees. By means of an additional significant dummy test, that shows an influence of the state of the forest (burned or unburned), this equation predicted the referenced biomass more accurately. The second equation consists of three lidar metrics variables: *INTP75*, *INTP80, PercAAL.* Most of the variables used in the equations are either connected to the height or some tree crown related parameters.

The not reflected tree trunks of the burned area did in the end not influence the analysis. Still it is notable that this behaviour of the reflectance gives some restrictions to the way burned and coaled surfaces and objects can be scanned with LiDAR technology.

With the lawnmower pattern of the scanning flights and a 50% overlap of the scan swath some parts of the scan had some inaccuracies. The overlap of the clouds at some point need to be solved by a better GPS positioning of the UAV. This could be achieved with integrating a simultaneous localization and mapping system (SLAM).

The potential connection between fire severity and a detected change in biomass was successful in this case. Even though the biomass loss was only related to needles, the fitting of the equation showed results, which can be helpful in further studies regarding the severity of fires and their biomass loss. With more advanced LiDAR scanning the results may be even improved.

For further studies it could be useful to generate DNBR maps of the forest area in Leiria to access data about the regeneration, the vegetation survival and possible delayed mortality.

References

Alcarva, Unidade. 2011. “Plano de Gestão Florestal - Mata Nacional De Leiria.” http://www2.icnf.pt/portal/florestas/gf/pgf/publicitacoes/encerradas/dcnf-centr/pgf-mn-leiria.

Alonzo, M., D. C. Morton, B. D. Cook, H. E. Andersen, C. Babcock, and R. Pattison. 2017. “Patterns of Canopy and Surface Layer Consumption in a Boreal Forest Fire from Repeat Airborne Lidar.” *Environmental Research Letters* 12 (6). https://doi.org/10.1088/1748-9326/aa6ade.

Andersen, H. E., R.J. McGaughey, and S. E. Reutebuch. 2005. “Estimating Forest Canopy Fuel Parameters Using LIDAR Data.” *Remote Sensing of Environment* 94 (4): 441–49. https://doi.org/10.1016/j.rse.2004.10.013.

André, J. N., and M. F. N. Cordeiro. 2016. “O Risco Da Mata Nacional de Leiria Passar a Ser Gerida Por Privados.” 2016. https://www.uc.pt/fluc/nicif/riscos/Documentacao/Congressos/Apresentacoes_ICI_VENR/30-Josse_Nunes_O_Risco_Mata_Nacional_Leiria.

Angelo, J. J., B. W. Duncan, and J. F. Weishampel. 2010. “Using Lidar-Derived Vegetation Profiles to Predict Time since Fire in an Oak Scrub Landscape in East-Central Florida.” *Remote Sensing* 2 (2): 514–25. https://doi.org/10.3390/rs2020514.

Bater, C., M. Wulder, J. White, and N. Coops. 2010. “Integration of LIDAR and Digital Aerial Imagery for Detailed Estimates of Lodgepole Pine (Pinus Contorta) Volume Killed by Mountain Pine Beetle (Dendroctonus Ponderosae).” *Journal of Forestry* 108 (April): 111–19.

Bishop, B. D., B. C. Dietterick, R. A. White, and T. B. Mastin. 2014. “Classification of Plot-Level Fire-Caused Tree Mortality in a Redwood Forest Using Digital Orthophotography and LiDAR.” *Remote Sensing* 6 (3): 1954–72. https://doi.org/10.3390/rs6031954.

Bright, B. C., J. A. Hicke, and A. T. Hudak. 2012. “Estimating Aboveground Carbon Stocks of a Forest Affected by Mountain Pine Beetle in Idaho Using Lidar and Multispectral Imagery.” *Remote Sensing of Environment* 124: 270–81. https://doi.org/10.1016/j.rse.2012.05.016.

Chen, Q. 2010. “Assessment of Terrain Elevation Derived from Satellite Laser Altimetry over Mountainous Forest Areas Using Airborne Lidar Data.” *ISPRS Journal of Photogrammetry and Remote Sensing* 65 (1): 111–22. https://doi.org/10.1016/j.isprsjprs.2009.09.004.

———. 2013. “LiDAR Remote Sensing of Vegetation Biomass.” *Remote Sensing of Natural Resources*, no. July 2013: 399–420. https://doi.org/10.1201/b15159.

Chu, T., and X. Guo. 2013. “Remote Sensing Techniques in Monitoring Post-Fire Effects and Patterns of Forest Recovery in Boreal Forest Regions: A Review.” *Remote Sensing*. https://doi.org/10.3390/rs6010470.

Chuvieco, E. 2008. “Earth Observation of Global Change: The Role of Satellite Remote Sensing in Monitoring the Global Environment.” *Earth Observation of Global Change: The Role of Satellite Remote Sensing in Monitoring the Global Environment* 89 (32): 1–223. https://doi.org/10.1007/978-1-4020-6358-9.

Chuvieco, E., M.P. Martin, and A. Palacios. 2010. “Assessment of Different Spectral Indices in the Red-near-Infrared Spectral Domain for Burned Land Discrimination, International Journal of Remote Sensing, 23:23, 5103-5110.” *International Journal of Remote Sensing*, no. March 2012: 37–41. https://sci-hub.tw/https://www.tandfonline.com/doi/abs/10.1080/01431160210153129.

Cocke, A. E., P. Z. Fulé, and J. E. Crouse. 2005. “Comparison of Burn Severity Assessments Using DNBR and Ground Data,” 189–98.

Core Team, R. 2016. “R: A Language and Environment for Statistical Computing. R Foundation for Statistical Computing, Vienna, Austria.” http://www.rstudio.com/.

Escuin, S., R. Navarro, and P. Fernández. 2008. “Fire Severity Assessment by Using NBR (Normalized Burn Ratio) and NDVI (Normalized Difference Vegetation Index) Derived from LANDSAT TM/ETM Images.” *International Journal of Remote Sensing* 29 (4): 1053–73. https://doi.org/10.1080/01431160701281072.

Faias, Sónia M. M. P. 2009. “Analysis of Biomass Expansion Factors for the Most Important Tree Species in Portugal.” Tese de Mestrado.

Fernández-Manso, A., O. Fernández-Manso, and C. Quintano. 2016. “SENTINEL-2A Red-Edge Spectral Indices Suitability for Discriminating Burn Severity.” *International Journal of Applied Earth Observation and Geoinformation* 50 (April): 170–75. https://doi.org/10.1016/j.jag.2016.03.005.

Fraser, R. H., J. Sluijs, and R. J. Hall. 2017. “Calibrating Satellite-Based Indices of Burn Severity from UAV-Derived Metrics of a Burned Boreal Forest in NWT, Canada.” *Remote Sensing* 9 (3). https://doi.org/10.3390/rs9030279.

García, M., D. Riaño, E. Chuvieco, and F. M. Danson. 2010. “Estimating Biomass Carbon Stocks for a Mediterranean Forest in Central Spain Using LiDAR Height and Intensity Data.” *Remote Sensing of Environment* 114 (4): 816–30.

https://doi.org/10.1016/j.rse.2009.11.021.

García, M., D. Riaño, E. Chuvieco, J. Salas, and F. M. Danson. 2011. “Multispectral and LiDAR Data Fusion for Fuel Type Mapping Using Support Vector Machine and Decision Rules.” *Remote Sensing of Environment* 115 (6): 1369–79. https://doi.org/10.1016/j.rse.2011.01.017.

Garcia, M., S. Saatchi, A. Casas, A. Koltunov, S. Ustin, C. Ramirez, J. Garcia-Gutierrez, and H. Balzter. 2017. “Quantifying Biomass Consumption and Carbon Release from the California Rim Fire by Integrating Airborne LiDAR and Landsat OLI Data.” *Journal of Geophysical Research: Biogeosciences* 122 (2): 340–53. https://doi.org/10.1002/2015JG003315.

Hudak, A.T., J. S. Evans, and A. M. S. Smith. 2009. “LiDAR Utility for Natural Resource Managers.” *Remote Sensing* 1 (4): 934–51. https://doi.org/10.3390/rs1040934.

“Humboldt State Geospatial Online.” 2014. 2014. http://gsp.humboldt.edu/olm_2015/Courses/GSP_216_Online/lesson5-1/NBR.html.

Jenkins, J. C., R. A. Birdsey, and Y. Pan. 2001. “Biomass and NPP Estimation for the Mid-Atlantic Region (USA) Using Plot-Level Forest Inventory Data.” *Ecological Applications* 11 (4): 1174–93. https://doi.org/10.1890/1051-0761(2001)011[1174:BANEFT]2.0.CO;2.

Kane, R., J. A. Lutz, S. L. Roberts, D. F. Smith, R. J. McGaughey, N. A. Povak, and M. L. Brooks. 2013. “Landscape-Scale Effects of Fire Severity on Mixed-Conifer and Red Fir Forest Structure in Yosemite National Park.” *Forest Ecology and Management* 287: 17–31. https://doi.org/10.1016/j.foreco.2012.08.044.

Keeley, J. 2009. “Fire Intensity , Fire Severity and Burn Severity : A Brief Review and Suggested Usage.” *International Journal of Wildland Fire* 18: 116–26. https://doi.org/10.1071/WF07049.

Korets, M., V. Ryzhkova, I. Danilova, A. Sukhinin, and S. Bartalev. 2010. “Forest Disturbance Assessment Using Satellite Data of Moderate and Low Resolution.” In *Advances in Global Change Research*, 40:3–19. https://doi.org/10.1007/978-90-481-8641-9_1.

Kronseder, K., U. Ballhorn, V. Böhmc, and F. Siegert. 2012. “Above Ground Biomass Estimation across Forest Types at Different Degradation Levels in Central Kalimantan Using Lidar Data.” *International Journal of Applied Earth Observation and Geoinformation* 18 (1): 37–48. https://doi.org/10.1016/j.jag.2012.01.010.

Kwak, D. A., J. Chung, W. K. Lee, M. Kafatos, Y. L. Si, H. K. Cho, and S. H. Lee. 2010. “Evaluation for Damaged Degree of Vegetation by Forest Fire Using Lidar and a Digital Aerial Photograph.” *Photogrammetric Engineering and Remote Sensing* 76 (3): 277–87.

https://doi.org/10.14358/PERS.76.3.277.

Lefsky, M. A., W. B. Cohen, G. G. Parker, and D. J. Harding. 2002. “Lidar Remote Sensing for Ecosystem Studies.” *BioScience* 52 (1): 19. https://doi.org/10.1641/0006-3568(2002)052[0019:lrsfes]2.0.co;2.

Longo, M., M. Keller, M. N. Dos-Santos, V. Leitold, E. R. Pinagé, A. Baccini, S. Saatchi, E. M. Nogueira, M. Batistella, and D. C. Morton. 2016. “Aboveground Biomass Variability across Intact and Degraded Forests in the Brazilian Amazon.” *Global Biogeochemical Cycles* 30 (11): 1639–60. https://doi.org/10.1002/2016GB005465.

Lu, D., Q. Chen, G. Wang, E. Moran, M. Batistella, M. Zhang, G. Vaglio Laurin, and D. Saah. 2012. “Aboveground Forest Biomass Estimation with Landsat and LiDAR Data and Uncertainty Analysis of the Estimates.” *International Journal of Forestry Research* 2012 (1): 1–16. https://doi.org/10.1155/2012/436537.

Lutes, D. C., R. E. Keane, J. F. Caratti, C. H. Key, N. C. Benson, S. Sutherland, and L. J. Gangi. 2006. “FIREMON: Fire Effects Monitoring and Inventory System. Gen. Tech. Rep. RMRS-GTR-164-CD,” no. June. https://doi.org/10.2737/RMRS-GTR-164.

Magdon, P., E. González-Ferreiro, C. Pérez-Cruzado, E. S. Purnama, D. Sarodja, and C. Kleinn. 2018. “Evaluating the Potential of ALS Data to Increase the Efficiency of Aboveground Biomass Estimates in Tropical Peat-Swamp Forests.” *Remote Sensing* 10 (9). https://doi.org/10.3390/rs10091344.

Marques, P. J. P. 2010. “Os Solos Da Mata Nacional De Leiria : Características E Classificação.” Tese de Mestrado.

McGaughey, B. 2018. “FUSION/LDV LIDAR Analysis and Visualization Software.” 2018. http://forsys.cfr.washington.edu/fusion/fusion_overview.html.

Miller, J. D., and A. E. Thode. 2007. “Quantifying Burn Severity in a Heterogeneous Landscape with a Relative Version of the Delta Normalized Burn Ratio (DNBR).” *Remote Sensing of Environment* 109 (1): 66–80. https://doi.org/10.1016/j.rse.2006.12.006.

Morgan, P., R. E. Keane, G. K. Dillon, T. B. Jain, A. T. Hudak, E. C. Karau, P. G. Sikkink, Z. A. Holden, and E. K. Strand. 2014. “Challenges of Assessing Fire and Burn Severity Using Field Measures, Remote Sensing and Modelling.” *International Journal of Wildland Fire* 23 (8): 1045–60. https://doi.org/10.1071/WF13058.

Parks, S. A., G. K. Dillon, and C. Miller. 2014. “A New Metric for Quantifying Burn Severity: The Relativized Burn Ratio.” *Remote Sensing* 6 (3): 1827–44. https://doi.org/10.3390/rs6031827.

Popescu, S. C. 2007. “Estimating Biomass of Individual Pine Trees Using Airborne Lidar.” *Biomass and Bioenergy* 31 (9): 646–55. https://doi.org/10.1016/j.biombioe.2007.06.022.

Riaño, D., E. Meier, B. Allgöwer, E. Chuvieco, and S. L. Ustin. 2003. “Modeling Airborne Laser Scanning Data for the Spatial Generation of Critical Forest Parameters in Fire Behavior Modeling.” *Remote Sensing of Environment* 86 (2): 177–86. https://doi.org/10.1016/S0034-4257(03)00098-1.

Roussel, J. 2019. “LidR Package.” https://www.rdocumentation.org/packages/lidR/versions/2.1.4.

RUS-Copernicus. 2017. “ACTIVE FIRE DETECTION WITH SENTINEL-3 SLSTR USING SNAP JUNE 2017 , PORTUGAL,” no. June.

Sato, L. Y., V. C. F. Gomes, Y. E. Shimabukuro, M. Keller, E. Arai, M. N. Dos-Santos, I. F. Brown, and L. E. O. e. C. de Aragão. 2016. “Post-Fire Changes in Forest Biomass Retrieved by Airborne LiDAR in Amazonia.” *Remote Sensing* 8 (10): 1–15. https://doi.org/10.3390/rs8100839.

Seielstad, C. A., and L. P. Queen. 2003. “Using Airborne Laser Altimetry to Determine Fuel Models for Estimating Fire Behavior.” *Journal of Forestry* 101 (4): 10–17. https://doi.org/10.1093/jof/101.4.10.

Sheridan, R. D., S. C. Popescu, D. Gatziolis, C. L. S. Morgan, and N. W. Ku. 2015. “Modeling Forest Aboveground Biomass and Volume Using Airborne LiDAR Metrics and Forest Inventory and Analysis Data in the Pacific Northwest.” *Remote Sensing* 7 (1): 229–55. https://doi.org/10.3390/rs7010229.

Smith, A. M.S., L. B. Lentile, A. T. Hudak, and P. Morgan. 2007. “Evaluation of Linear Spectral Unmixing and DNBR for Predicting Postfire Recovery in a North American Ponderosa Pine Forest.” *International Journal of Remote Sensing* 28 (22): 5159–66. https://doi.org/10.1080/01431160701395161.

Smith, A M S, N A Drake, M J Wooster, A T Hudak, Z A Holden, and C J Gibbons. 2007. “Production of Landsat ETM+ Reference Imagery of Burned Areas within Southern African Savannahs: Comparison of Methods and Application to MODIS.” *International Journal of Remote Sensing* 28 (12): 2753–75. https://doi.org/10.1080/01431160600954704.

Stein, S.M., S. J. Comas, J.P. Menakis, M.A. Carr, S.I. Stewart, H. Cleveland, L. Bramwell, and V.C. Radeloff. 2013. “Wildfire, Wildlands, and People: Understanding and Preparing for Wildfire in the Wildland-Urban Interface - a Forests on the Edge Report. Gen. Tech. Rep. RMRS-GTR-299. Fort Collins, CO. U.S. Department of Agriculture, Forest Service,

Rocky Mountain Resear," no. January: 36.

Steinhorst, R. K., and R. H. Myers. 1988. "Classical and Modern Regression With Applications." *Journal of the American Statistical Association* 83 (401): 271. https://doi.org/10.2307/2288958.

Thomas, D., D. Butry, S. Gilbert, D. Webb, and J. Fung. 2017. "The Costs and Losses of Wildfires: A Literature Survey (NIST Special Publication 1215)." https://doi.org/10.6028/NIST.SP.1215.

Wulder, M. A., J. C. White, F. Alvarez, T. Han, J. Rogan, and B. Hawkes. 2009. "Characterizing Boreal Forest Wildfire with Multi-Temporal Landsat and LIDAR Data." *Remote Sensing of Environment* 113 (7): 1540–55. https://doi.org/10.1016/j.rse.2009.03.004.

Zwally, H. J., B. Schutz, W. Abdalati, J. Abshire, C. Bentley, A. Brenner, J. Bufton, et al. 2002. "ICESat's Laser Measurements of Polar Ice, Atmosphere, Ocean, and Land." *Journal of Geodynamics* 34 (3–4): 405–45. https://doi.org/10.1016/S0264-3707(02)00042-X.

Appendix

Equation fitting output

Equation 10

lm(formula = sqrt (Biomass) ~ HTmax + (HTkurt + P80) * state

Residuals:	Min	1Q	Median	3Q	Max
	-0.70964	-0.31463	0.08692	0.20087	0.71297

Coefficients:	Estimate	Std. Error	t value	Pr(>|t|)	
(Intercept)	-54.7964	13.98712	-3.918	0.003524	**
HTmax	-0.43053	0.10491	-4.104	0.002661	**
HTkurt	0.20532	0.06099	3.366	0.008305	**
P80	3.21581	0.5887	5.463	0.000399	***
stateU	57.87677	14.56921	3.973	0.003242	**
HTkurt:stateU	0.67376	0.11613	5.802	0.000259	***
P80:stateU	-2.46241	0.5836	-4.219	0.002242	**

Residual standard error:	0.5537	on 9 degrees of freedom
Multiple R-squared:	0.9381	
Adjusted R-squared:	0.8968	
F-statistic:	22.72	on 6 and 9 DF
p-value:	5.896e-05	

Plot	Subplot	HTmax	HTkurt	P80
P1B	1B1	28.01	10.77	23.74
	1B2	25.33	29.86	22.52
	1B3	25.95	18.41	23.02
	1B4	24.85	21.11	22.15
P1U	1U1	31.26	7.20	22.96
	1U2	26.86	2.84	24.02
	1U3	26.37	3.01	23.01
	1U4	28.40	1.14	24.94
P2B	2B1	29.64	1.41	25.04
	2B2	31.25	1.08	25.07
	2B3	30.56	1.12	25.20
	2B4	28.91	1.10	24.80
P2U	2U1	29.05	2.43	26.53
	2U2	33.69	3.74	26.60
	2U3	29.84	3.21	26.35
	2U4	30.06	7.77	27.66
	Minimum	24.85	1.08	22.15
	Maximum	33.69	29.86	27.66
	Mean	28.98	3.11	24.87

Equation 11

lm(formula	=	sqrt (Biomass) ~ INTP75 + (INTP80 + PercAAL) * state				
Residuals:	Min	1Q	Median	3Q	Max	
	-0.78836	-0.26395	0.06378	0.20134	0.7994	
Coefficients:	Estimate	Std. Error	t value	Pr(>|t|)		
(Intercept)	11.02175	4.75036	2.32	0.04547	*	
INTP75	1.34501	0.37683	3.569	0.00603	**	
INTP80	-1.34666	0.36412	-3.698	0.00493	**	
PercAAL	0.12117	0.05126	2.364	0.04233	*	
stateU	15.02894	6.53933	2.298	0.04714	*	
INTP80:stateU	-1.00996	0.26374	-3.829	0.00403	**	
PercAAL:stateU	0.15765	0.05873	2.684	0.02503	*	
Residual standard error:	0.5764	on 9 degrees of freedom				
Multiple R-squared:	0.9329					
Adjusted R-squared:	0.8882					
F-statistic:	20.85	on 6 and 9 DF				
p-value:	8.39E-05					

Plot	Subplot	INTP75	INTP80	PercAAL
P1B	1B1	25.00	26.00	14.85
	1B2	22.00	23.00	21.54
	1B3	23.00	24.00	17.55
	1B4	21.00	23.00	18.62
P1U	1U1	25.00	26.00	55.79
	1U2	24.00	25.00	44.70
	1U3	25.00	26.00	46.97
	1U4	23.00	24.00	36.67
P2B	2B1	20.00	21.00	31.67
	2B2	22.00	24.00	29.60
	2B3	18.00	19.00	35.04
	2B4	19.00	20.00	28.52
P2U	2U1	23.00	25.00	51.86
	2U2	26.00	28.00	60.87
	2U3	23.00	24.00	45.04
	2U4	24.00	25.00	64.89
	Minimum	18.00	19.00	14.85
	Maximum	26.00	28.00	64.89
	Mean	23.00	24.00	35.86

Biomass estimates based on inventory data

	Weight complete [kg/400m²]	Weight minus stem [kg/400m²]	Complete [t/ha] (>1m)	Without stem [t/ha] (>18,5m)
1B1	4999,59	609,83	124,99	15,25
1B2	6810,21	920,68	170,26	23,02
1B3	5357,11	724,46	133,93	18,11
1B4	4205,43	582,09	105,14	14,55
1U1	7155,63	1195,47	178,89	29,89
1U2	5429,67	932,36	135,74	23,31
1U3	5450,14	939,74	136,25	23,49
1U4	5156,46	873,61	128,91	21,84
2B1	7446,08	933,74	186,15	23,34
2B2	5663,31	720,47	141,58	18,01
2B3	7143,23	932,36	178,58	23,31
2B4	7165,19	905,59	179,13	22,64
2U1	6449,16	1010,58	161,23	25,26
2U2	5871,03	940,98	146,78	23,52
2U3	5950,81	876,54	148,77	21,91
2U4	12896,52	2048,35	322,41	51,21